

Recent Developments in Theory for W7-X

J. NÜHRENBURG, M. DREVLAK, R. HATZKY, R. KLEIBER, A. KÖNIES,
P. MERKEL, D. MONTICELLO⁺, C. NÜHRENBURG, A. REIMAN⁺, T.M. TRAN^{*}

Max-Planck-Institut für Plasmaphysik, EURATOM Association, jun@ipp.mpg.de

^{*}Centre de Recherches en Physique des Plasmas, Association Euratom-Confédération Suisse,
Ecole Polytechnique Fédérale de Lausanne, PPB, 1015 Lausanne, Switzerland

⁺ Princeton Plasma Physics Laboratory, PO Box 451, Princeton, NJ 08543-0451, USA

Abstract

The Stellarator Theory Division at the Greifswald Branch has been concentrating on widening the scope of theoretical work related to W7-X. Some of such areas are the quality of finite- β magnetic surfaces, energetic-particle-driven Alfvén eigenmode, resistively driven drift and ion-temperature-gradient-driven instabilities. New results pertaining to these issues are: i) MHD GAEs in W7-X-type equilibria are discovered and the first 3d drift-kinetic formulation of interaction with energetic particles is developed as nonlinear eigenvalue problem analytically and computationally; ii) for the first time, mode structures of globally calculated resistive drift instabilities with poloidal mode numbers of $O(10^3)$ and exhibiting the relative importance of toroidal vs. helical coupling are obtained in a toroidal stellarator; iii) for the first time, nonlinear saturation levels of kinetic ITG modes are obtained with energy conservation in a θ -pinch, iv) fixed-boundary-PIES W7-X-type high- β equilibria - well converged on an NEC-SX5 - show even 5/5 islands to be very thin.

1. Global Ideal MHD for 3-D Equilibria

The CAS3D 3-d ideal MHD stability code [1] has been applied to investigating the stable part of the ideal MHD spectrum, in particular to understanding gap formation and the structure of global, stable modes, as they are possible candidates for destabilization by α -particles.

Using CAS3D the standard tokamak picture with geometry-induced gaps and modes, e.g. TAEs and EAEs, and β -induced gaps and modes has been extended by the stellarator-type gaps and

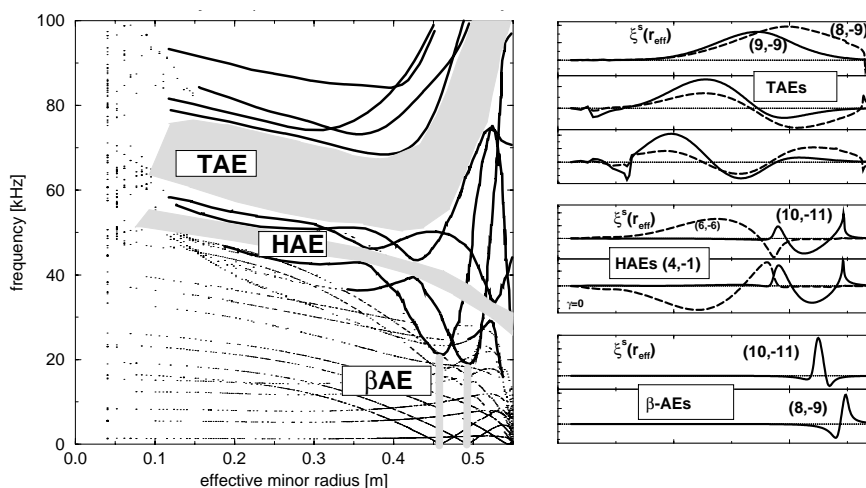


Figure 1: Ideal continuous MHD spectrum (left frame) for the W7-X standard high- ν case (five field periods, $\langle\beta\rangle \approx 0.05$, $\nu \gtrsim 1$). Lines represent the continua (solid: Alfvén, dotted: slow). The prominent spectral gaps are indicated by shading. The β AEs (bottom right frame for the dominant harmonics of their normal displacements versus effective minor radius) occur at 16.1 kHz and 16.8 kHz, helicity-induced global modes (middle right) at 31 kHz (even) and 33 kHz (odd); an anti-Sturmian set of TAEs (top right) around 60 kHz. CAS3D code, $N = 1$ mode family, 288 radial mesh points, 15 perturbation harmonics, adiabatic index $\gamma = 5/3$ ($=0$ for middle right frame). Normalization: $B = 2.5\text{T}$, $n_0 = 3 \cdot 10^{20}\text{m}^{-3}$.

modes originating from purely stellarator-type couplings, e.g. helicity and mirror fields giving rise to HAEs and MAEs. Together with the 3-d analog of the cylindrical GAE [2] for which the frequency appears just below the corresponding Alfvén continuum in case of sufficiently low shear, the stellarator, in principle, leads to a greater variety of global, stable modes. In the W7-X high- ι high-mirror variant [3] GAEs were not detected, since the corresponding continuum extrema are not sufficiently flat. For the frequency ranges and locations of the β -, toroidicity- and helicity-induced gaps and modes see Fig. 1.

2. Fast Particle Effects

The gap eigenmodes of the Alfvén spectrum may be destabilized by energetic particles. To account for kinetic effects a linearized drift kinetic equation has been solved in three-dimensional geometry with both reflected and passing particles [4]. The radial particle drifts away from the flux surface have been neglected. Therefore, a flux surface is a constant of the particle motion and approximates the drift surface which is given by the constancy of the second adiabatic invariant. This approximation is in particular suitable in the W7-X case where the radial particle drift has been minimized [5]. For the orbit integration a propagator technique [6] is used allowing the expansion around bounce averaged toroidal and poloidal drifts, which neglects side band coupling introduced by the spatial dependence of the particle drift frequencies.

From the force balance equation

$$\vec{\nabla} \cdot \vec{P} = \rho_q \vec{E} + \vec{j} \times \vec{B}$$

with MHD-like perturbations

$$\vec{B}^{(1)} = \vec{\nabla} \times (\vec{\xi}_\perp \times \vec{B}), \quad \vec{A}^{(1)} = \vec{\xi}_\perp \times \vec{B}, \quad \vec{E}^{(1)} = -i\omega \vec{A}^{(1)}, \quad \phi = \phi^{(1)} = 0$$

a generalized energy integral can be obtained. Here, the fluid compression term of ideal MHD is replaced by a kinetic term for each particle species which contains the resonant interaction of the mode with particle drift or bounce frequencies, resp.

$$\delta W_{kin}^{MHD} = \delta W_{mag}^{MHD} + \delta W_{particle}$$

with

$$\begin{aligned} \delta W_{particle} = & \sum_{e,i,hot} \frac{\pi}{M^2} \sum_{\sigma} \sigma \int d^3x \int d\Gamma \sum_{\substack{n,m \\ n',m'}} \sum_{p=-\infty}^{\infty} \times \\ & \times \left(\frac{\partial F}{\partial \varepsilon} \right)_{\mu} \frac{\omega - (nJ - mI)\omega^*}{p\omega_c - m\sigma \langle \omega_d^\psi \rangle - n\sigma \langle \omega_d^\phi \rangle + \omega} \times \\ & \times e^{-im'\theta} L_{m'n'}^{(1)*} \left\langle e^{i[(p-n'-vm')\phi - S(\phi)]} \right\rangle \times \\ & \times e^{im\theta} L_{mn}^{(1)} \left\langle e^{-i[(p-n-vm)\phi - S(\phi)]} \right\rangle \end{aligned}$$

with the bounce-averaged drift frequencies $\langle \omega_d \rangle$, the reflection or transition frequency ω_c , the diamagnetic drift ω^* , $F(s, \varepsilon, \mu)$ the distribution function, $L^{(1)}$ the perturbed particle Lagrangian, σ the direction of particle motion, M the species mass and S a function resulting from the propagator [4]. Obviously, the according eigenvalue problem is nonlinear and involves a fivefold integration over phase space for the calculation of the matrix elements.

3. Global Resistive Drift Modes in General Geometry

Contrary to former studies of drift waves [7] - [11], which always employed the ballooning transformation to reduce the three-dimensional equations to an eigenvalue problem along the field line, one can choose the more difficult global approach, i.e. to solve the three-dimensional eigenvalue problem inside a toroidal shell without any approximations regarding the mode structure. Since here effects of the equilibrium geometry are the main aim, one can start with simplified equations including just as much physics as necessary for obtaining instability but making no approximations regarding the geometry and allow for general three-dimensional equilibria. Using the linearized Braginskii-equations with the temperature equations neglected, the following assumptions are utilized: Ions are treated as a cold fluid, resistivity is included in the parallel components and perturbations are regarded as electrostatic. This gives

$$\begin{aligned} \omega \frac{\tilde{n}}{n} + iA(L_c + L_d)\tilde{\Phi} - \frac{\omega A^2}{B^2} \nabla \nabla_{\perp} \tilde{\Phi} + \frac{1}{\omega} \nabla \nabla_{\parallel} \frac{\tilde{n}}{n} &= 0 \\ \omega \frac{\tilde{n}}{n} + iA(L_c + L_d)\tilde{\Phi} - iA \frac{1}{n} L_c \tilde{n} + iC \nabla \nabla_{\parallel} (\tilde{\Phi} - \frac{\tilde{n}}{n}) + \frac{1}{\omega} \nabla \nabla_{\parallel} \frac{\tilde{n}}{n} &= 0 \end{aligned}$$

for the density and potential perturbation. The dimensionless quantities A , C describe inertia length and resistivity, the operators L_c , L_d represent curvature and diamagnetic velocity. Normally the last term on the left-hand sides was neglected (i.e. neglect of sound wave effects); including these terms in the calculations shows that this is indeed justified.

To allow for general three-dimensional equilibria – which e.g. can be calculated by the VMEC code – all the operators are expressed in magnetic (Boozer) coordinates (s, ϑ, φ) .

For solving the equations the perturbations are Fourier decomposed in the angle-like variables; radially finite differences of second order are used. In order to make possible the treatment of high mode numbers a phase-factor transformation (M_P, N_P) is introduced. The resulting generalized complex eigenvalue problem with non-hermitian matrices is solved by an Implicitly Restarted Arnoldi Method.

To check the code a simple analytical axially symmetric model was employed with various rotational transforms typical of a tokamak or a stellarator. The eigenvalues (for different phase factors) calculated with the global code were in good agreement with those obtained by using a simple ballooning approach. For positive ι it is possible to find modes with the global code which could not be found by the ballooning approach. In general, increasing ι or changing ι' from negative to positive has led to a considerable decrease in the growthrate.

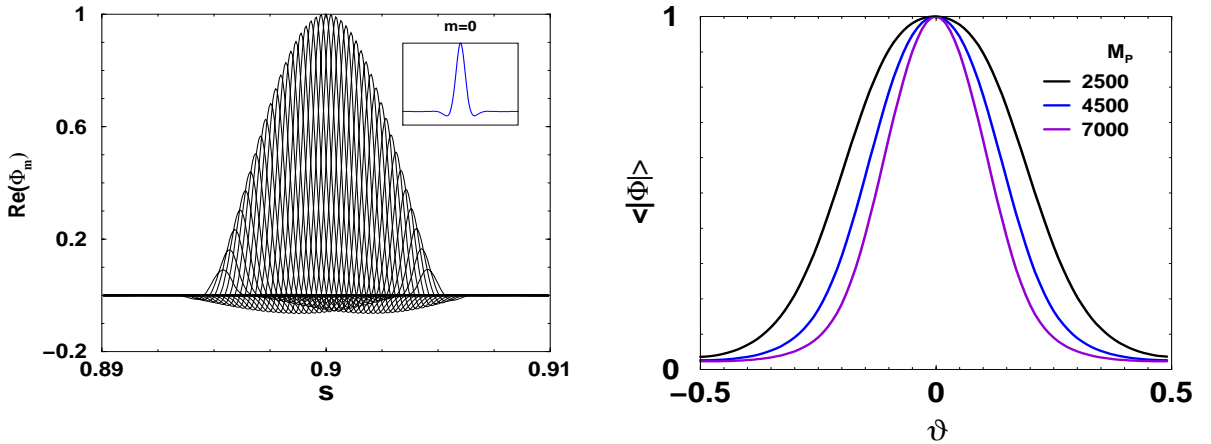


Figure 2: Real part of the eigenfunction for $M_P = 4500$ (left) and radially averaged mode-amplitude (right). $\text{Im}(\omega) = 1.4$. The insert shows the $m=0$ component.

Results obtained with the global code for VMEC generated tokamak and stellarator equilibria are presented in the Figures. Figure 2 displays the result of a calculation for a circular tokamak with $A = 10$, $\beta = 0$ and $\iota(s) = 0.333 - 0.333(s - 0.9)$. The eigenfunction is composed of peaks centered around the respective resonant surface. The averaged mode amplitude shows a strong ballooning effect at the low field side ($\vartheta = 0$) of the torus. The same tokamak with a W7-X-like $\iota(s) = 0.95 + 0.35(s - 0.9)$ gives a totally different mode structure (Fig.3) where the mode maximum need not be located at the low field region.

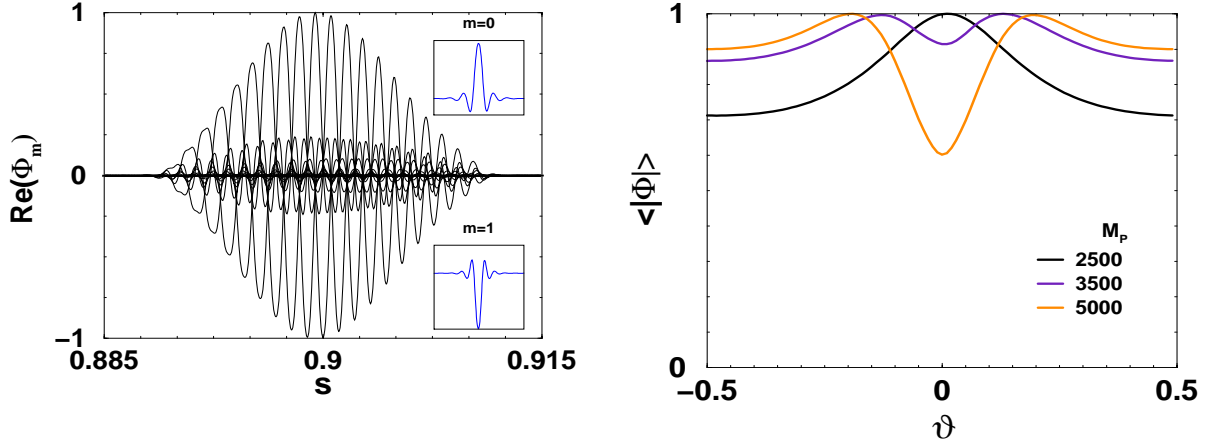


Figure 3: Real part of the eigenfunction for $M_P = 5000$ (left) and radially averaged mode-amplitude (right). $\text{Im}(\omega) = 0.55$.

Figure 4 displays the mode structure on a flux surface ($s = 0.9$) for $M_P = 7000$ calculated for a straight $\ell=2$ -stellarator with one field period and ellipticity $\delta = 0.3$. The mode is essentially slab like (because of the small shear) with small helical components. For very high M_P (e.g. $2 \cdot 10^4$) the mode maximum shifts from the low to the high field region.

The eigenmode ($M_P = 5000$) for a toroidal $\ell=2$ -stellarator with five field periods, $\delta = 0.3$ and $A = 10$ is shown in Fig.5. The pronounced maximum at $\vartheta=0$ is caused by the toroidal coupling; the smaller variation results from the helical coupling.

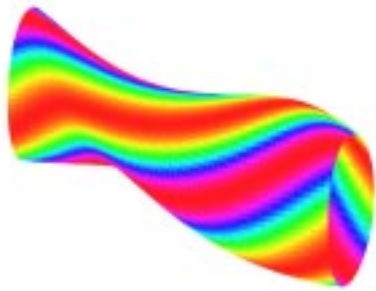


Figure 4: $|\tilde{\Phi}(s=0.9)|$ in real space. $\text{Im}(\omega) = 0.67$. Red corresponds to a maximum, orange to a minimum.

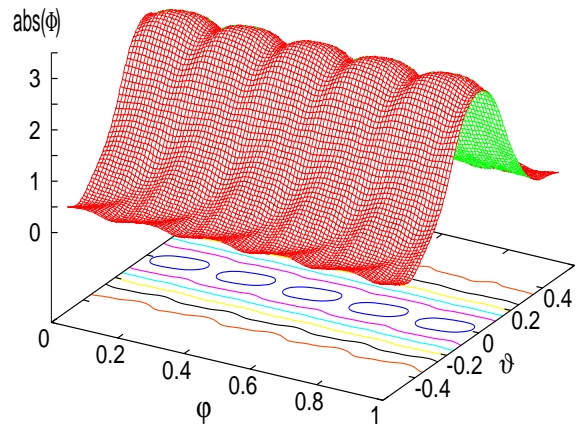


Figure 5: $|\tilde{\Phi}(s=0.9)|$ in magnetic coordinates. $\text{Im}(\omega) = 1.3$.

These results show that the developed code can be used to investigate resistive drift modes in three-dimensional equilibria. The next step will be to search for such modes in W7-X with its very different coupling structure.

4. Energy Conservation for a Nonlinear Simulation Code for ITG Modes

ITG instabilities are now commonly held responsible for turbulence giving rise to anomalous ion heat transport in the core of tokamaks. ITG turbulence could become the dominant transport mechanism of W7-X as collisional transport has been optimized in this stellarator. Therefore a nonlinear 3D global gyrokinetic simulation code for W7-X has to be developed. First results with linear simulations of 3D magnetic configurations have already been achieved [12] while nonlinear simulations with energy conserving properties are still under development.

The global nonlinear simulations are very demanding with respect to the numerical methods and the computational effort. Although the underlying set of gyrokinetic equations is energy-conserving, energy conservation is usually lost in the saturation phase [13].

In a first step, we reduce the problem to a geometrically simple configuration: the θ -pinch; in the simplest case with $\beta = 0$: $\mathbf{B} = B_0 \mathbf{e}_z$.

For this purpose we adapted the nonlinear particle-in-cell (PIC) code ORB [13] to handle a plasma in the θ -pinch configuration. The adapted ORB code, which will be stated as TORB further on, is able to make a global 3D simulation of the nonlinear time evolution of the ITG turbulence.

The gyrokinetic model

The nonlinear gyrokinetic equations as derived in [14] are used to calculate the time evolution of the ion guiding center distribution function $f(\mathbf{R}, v_{\parallel}, \tilde{\mu})$:

$$\frac{\partial f}{\partial t} + \frac{d\mathbf{R}}{dt} \cdot \nabla f + \frac{dv_{\parallel}}{dt} \frac{\partial f}{\partial v_{\parallel}} = 0 \quad \text{where} \quad \tilde{\mu} \stackrel{\text{def}}{=} \frac{v_{\perp}^2}{2B}, \quad \frac{d\tilde{\mu}}{dt} \stackrel{!}{=} 0$$

The equations of motion for the perturbed guiding center trajectories of the ions in reduced phase space ($\mathbf{R}, v_{\parallel}, \tilde{\mu}$ here) are:

$$\frac{d\mathbf{R}}{dt} = v_{\parallel} \mathbf{e}_z + \frac{1}{B_0} \langle \mathbf{E} \rangle \times \mathbf{e}_z \quad \frac{dv_{\parallel}}{dt} = \frac{q_i}{m_i} \mathbf{e}_z \cdot \langle \mathbf{E} \rangle$$

where q_i and m_i are the ion charge and mass.

The quasi-neutrality equation to calculate the electrostatic potential ϕ to $O((k_{\perp} \rho_i)^2)$ is derived from [14] by assuming Boltzmann electrons and quasi-neutrality

$$\langle n_i \rangle(\mathbf{x}, t) - n_0(r) = \frac{en_0(r)}{k_B T_e(r)} [\phi(\mathbf{x}, t) - \bar{\phi}(r, \theta, t)] - \nabla_{\perp} \cdot \left(\frac{n_0(r, t)}{B_0 \Omega_i(\mathbf{x})} \nabla_{\perp} \phi(\mathbf{x}, t) \right)$$

with the gyro-averaged ion density $\langle n_i \rangle$, the background density of the Maxwellian distribution function n_0 , the electron temperature T_e , the average of the potential over a field line $\bar{\phi}$ and the cyclotron frequency $\Omega_i = q_i/m_i B$. In the current version of the TORB code, the subtraction of the potential average $\bar{\phi}$ is not implemented yet. Further, we define the kinetic energy E_{kin} and the electrostatic energy E_{field} as:

$$E_{\text{kin}} \stackrel{\text{def}}{=} \int m_i \left(\tilde{\mu} B + \frac{v_{\parallel}^2}{2} \right) f d\mathbf{R} dv \quad \text{and} \quad E_{\text{field}} \stackrel{\text{def}}{=} \frac{q_i}{2} \int (\langle n_i \rangle - n_0) \phi d\mathbf{x}$$

It can be shown that the total energy $E_{\text{tot}} = E_{\text{kin}} + E_{\text{field}}$ is conserved for the set of equations used here.

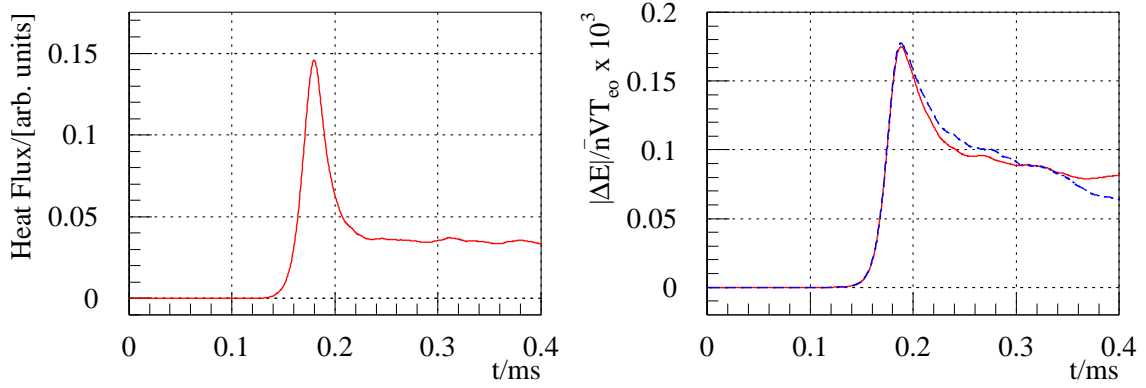


Figure 6: Left: Averaged radial heat flux over time. Right: Absolute values of the changes in kinetic energy (dashed line) and electrostatic field energy (solid line) over time.

Numerical methods

The TORB code uses a δf [13] method for the discretization of the ion guiding center distribution function f so that tracer resolution is not wasted to represent the background Maxwellian distribution function f_0 and its gradient. Finite elements are chosen to represent both the electrostatic field ϕ and the tracer shape (cloud-in-cell) which already has been successful in linear ITG simulations [15]. The whole gyro-averaging process for the charge-assignment and the electric field \mathbf{E} [16] is not limited by any $k_{\perp}\rho_i$ expansion. It is only limited by the resolution of the grid and its finite element basis. It has a positive numerical effect because it acts as a $k_{\perp}\rho_i$ filter, hence smoothing higher fluctuations.

The charge-assignment has the principal disadvantage to produce noise due to statistical error. For that reason, after charge-assignment a Fourier-filter is applied to diminish the high mode numbers on the grid. The noise is strongly influenced by the number of tracers per grid cell and by the initial distribution of the tracers in reduced phase space. To minimize the statistical error, all the tracers should have about the same weight w_p during the simulation. Therefore the following iteration is performed: in a first step a simulation is run to obtain the distribution of tracers in phase space; in a second step this information is used to initially distribute the tracers in phase space where they are really needed.

Results

The following physical parameters have been used:

Deuterium, $B_0 = 2.5$ T, $T_i(s_0) = T_e = 5$ keV where $s = r/r_a$, aspect ratio $A = R_0/r_a = 10$ with $r_a/\rho_i = 135 \Rightarrow$ cylinder length $L_z/\rho_i = 2\pi R_0/\rho_i = 8456$, flat density profile $n_0 \Rightarrow L_n = 1/|\nabla \ln n_0| = \infty$, $d \ln T_i/ds$ profile peaking at $s_0 = 0.5$ and $L_T(s_0) = 1/|\nabla \ln T_i| = 1/3r_a$.

The following numerical parameters are used: a cubic spline finite element grid for the discretization of the electrostatic potential with $n_r = 64$, $n_{\theta} = 128$ and $n_z = 32$, a total number of $N = 2^{26}$ tracers, a Fourier filtering in (θ, z) keeping only the $-24 \leq m \leq 24$ poloidal and $0 \leq n \leq 6$ toroidal modes and a time step in the linear phase of $\Omega_i \Delta t = 200$ and in the nonlinear phase of $\Omega_i \Delta t = 50$.

The result of the nonlinear simulation can be seen in Fig. 6. On the left side the averaged radial heat flux is shown over time. After the peak at $t = 0.19$ ms it reaches a nearly constant value without showing any influence of numerical noise. On the right side the absolute values of $\Delta E_{\text{kin}} = E_{\text{kin}}(t) - E_{\text{kin}}(t_0)$ and E_{field} are seen to be nearly identical until the peak reaches its maximum. In the saturation phase, energy conservation is, in contrast to previous results, violated only slightly (less than 20%).

Thus, it is possible to achieve acceptable energy conservation for a 3D ITG turbulence simulation using a PIC code. As a next step the cylindrical configuration will be modified to more elaborated configurations.

5. Fixed Boundary Equilibria with Islands for W7-X

The PIES (Princeton Island Equilibrium Solver) code ([17] - [21]) solves the magnetohydrostatic equilibrium equations with the help of a Picard iteration of the fields,

$$\nabla \times \vec{B}^{n+1} = \vec{J}(\vec{B}^n).$$

In order to establish convergence, new field quantities are blended with those of the previous iteration. The algorithm may require very large values of the blending parameter $0 < b < 1$, for instance $b = 0.99$, to guarantee stability of the iteration. As a consequence, many iterations must be performed before the solution is approximated with satisfactory accuracy.

Significant acceleration of convergence is achieved by using periodic sequences of blending parameters instead of a constant one. Here, subsequent values of b , b_v , are chosen as

$$b_v = 1 + (b^{(0)})/x_v,$$

where x_v are the zeroes of a Chebyshev polynomial. This method results in better damping of the error of the solution. ([22], [23]).

The PIES code was used in fixed-boundary calculations of equilibria in the neighborhood of W7-X. Starting from the original configuration, only the coefficients (1,1) and (3,4) were modified so that the resonance $\iota = \frac{5}{3}$ is shifted into the volume between plasma axis and plasma edge. The computations started from fixed-boundary equilibria obtained with VMEC ([24], [25]). At large iteration counts a solution is approximated with very good accuracy and shows very small $\frac{5}{3}$ -islands. Figure 7 show as an example a case with $\langle \beta \rangle \sim 4.5\%$. The smooth rotational transform profile reflects the small size of the islands.

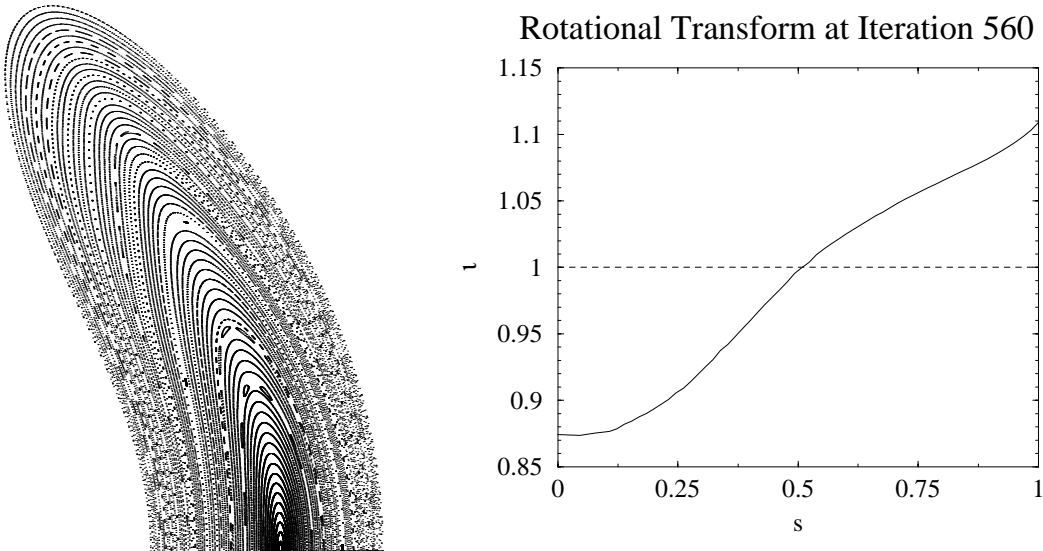


Figure 7: Poincaré plots of the magnetic field after 560 iterations (left) and final profile of the rotational transform (right).

A new blending scheme was developed in which the currents are exempt from blending. The initial error, associated with large islands occurring in the first iteration is reduced. As a consequence the solution can be obtained with fewer iterations.

6. Outlook

The Stellarator Theory Division in Greifswald is investigating various advanced (i. e. not considered in its original design) physical topics relevant for W7-X with the aim of understanding α -particle driven instabilities, turbulence at the plasma edge/core and the topology of finite- β equilibria with islands.

References

- [1] C. Nührenberg, Phys. Plasmas **6**, 137 (1999).
- [2] K. Appert et al., Plasma Phys. **24**, 1147 (1982).
- [3] C. Nührenberg, Phys. Plasmas **3**, 2401 (1996).
- [4] A. Könies, Phys. Plasmas **7**, 1139 (2000).
- [5] W. Lotz, J. Nührenberg, and C. Schwab, in Plasma Physics and Controlled Fusion Research, 1990, Nucl. Fusion Suppl. 1991 (International Atomic Energy Agency, Vienna, 1991), Vol. 2, pp. 603–611.
- [6] S. Brunner, J. Vaclavik, Phys. Plasmas **5**, 3929 (1998).
- [7] A. Bhattacharjee et al., Phys. Fluids **26**, 880 (1983).
- [8] N. Dominguez, B.A. Carreras, V.E. Lynch: Phys. Fluids B **4**, 2894 (1992).
- [9] R.E. Waltz, A.H. Boozer, Phys. Fluids B **5**, 2201 (1993).
- [10] M. Persson, J.L.V. Lewandowski, H. Nordmann, Phys. Plasmas **3**, 3720 (1996).
- [11] M. Persson et al., Plasma Phys. Control. Fusion **42**, 217 (2000).
- [12] Jost, G. et al., in Theory of Fusion Plasmas, Int. Workshop, Varenna, in press, (2000).
- [13] Tran, T. M. et al., in Theory of Fusion Plasmas, Int. Workshop, Varenna, p. 45–58, (1999).
- [14] Hahm, T. S., Phys. Fluids **31**, 2670 (1988).
- [15] Fivaz, M. et al., Comp. Phys. Comm. **111**, 27 (1998).
- [16] Hatzky, R. et al., in Theory of Fusion Plasmas, Int. Workshop, Varenna, in press, (2000).
- [17] A. H. Reiman, H. Greenside, Comput. Phys. Comm. **43**, 157 (1986).
- [18] A. H. Reiman, H. Greenside, J. Comput. Phys. **75**, 423 (1988).
- [19] H. S. Greenside et al., J. Comput. Phys. **81**, 102 (1989).
- [20] A. H. Reiman, H. Greenside, J. Comput. Phys. **87**, 349 (1990).
- [21] A. H. Reiman, N. Pomphrey, J. Comput. Phys. **94**, 225 (1991).
- [22] R. Chodura, A. Schlüter, J. Comput. Phys **41**, 68 (1981).
- [23] S. Arndt et al., Phys. Plasmas, **6** 1246 (1999).
- [24] S. P. Hirshman, J. C. Whitson, Phys. Fluids **26**, 3553 (1983).
- [25] S. P. Hirshman, K. Meier, Phys. Fluids **28**, 1387 (1985).